J Appl Electrochem (2013) 43:191–197
DOI 10.1007/s10800-012-0506-1

ORIGINAL PAPER

Spray-deposited NiO_x films on ITO substrates as photoactive electrodes for *p*-type dye-sensitized solar cells

Muhammad Awais · Denis D. Dowling · Mahfujur Rahman · Johannes G. Vos · Franco Decker · Danilo Dini

Received: 31 July 2012 / Accepted: 5 November 2012 / Published online: 30 November 2012

Abstract Spray deposition followed by sintering of nickel oxide (NiO_x) nanoparticles (average diameter: 40 nm) has been chosen as method of deposition of mesoporous NiO_x coatings onto indium tin oxide (ITO) substrates. This procedure allows the scalable preparation of NiO_x samples with large surface area ($\sim 10^3$ times the geometrical area) and its potential for applications such as electrocatalysis or electrochemical solar energy conversion, which require high electroactivity in confined systems. The potential of these NiO_x films as semiconducting cathodes for dye-sensitized solar cell (DSC) purposes has been evaluated for 0.3–3-μm-thick films of NiO_x sensitized with erythrosine B (ERY). The electrochemical processes involving the NiO_x coatings in the pristine and sensitized states were examined and indicated surface confinement as demonstrated by the linear dependence of the current densities with the scan rate of the cyclic voltammetry. Cathodic polarization of NiO_x on ITO can also lead to the irreversible reduction of the underlying ITO substrate because of the mesoporous nature of the sintered NiO_x film that allows the shunting of ITO to the electrolyte. ITO-based reduction processes alter irreversibly the properties of charge transfer through the ITO/NiO_x interface and limit the range of potential to NiO_x coatings sintered for DSC purposes.

Keywords Nickel oxide · p-Type semiconductor electrode · Semiconductor electrochemistry · Dye-sensitized solar cell · Indium tin oxide · Sintering

Electronic supplementary material The online version of this article (doi:10.1007/s10800-012-0506-1) contains supplementary material, which is available to authorized users.

M. Awais · D. D. Dowling · M. Rahman · J. G. Vos · D. Dini
Solar Energy Conversion Strategic Research Cluster, Dublin, Ireland

M. Awais
Interdisciplinary Research Centre in Biomedical Materials (IRCBM), COMSATS Institute of Information Technology (CIIT), Defence Road, Off Raiwind Road, Lahore, Pakistan

D. D. Dowling
School of Mechanical and Materials Engineering, University College Dublin, Dublin, Ireland

M. Rahman
School of Chemical and Bioprocess Engineering, University College Dublin, Dublin, Ireland

J. G. Vos
School of Chemical Sciences, Dublin City University, Dublin, Ireland

F. Decker · D. Dini (✉)
Department of Chemistry, University of Rome "La Sapienza", P.le Aldo Moro 5, 00185 Rome, Italy
e-mail: danilo.dini@uniroma1.it

1 Introduction

Nickel oxide (NiO_x with $1 < x < 1.5$) is a p-type semiconductor with wide band-gap ($E_g > 3.50$ eV), displaying room temperature conductivity values in the order of 10^{-4}–10^{-2} S cm^{-1} [1]. The intrinsic p-type conductivity of NiO_x is mainly related to its non-stoichiometric nature where Ni^{3+} centers constitute the oxide defects through which holes are transferred [2]. Moreover, the oxide is characterized by high chemical stability and optical transparency when in the configuration of thin film with thickness $l < 2$ μm [3, 4]. Because of this interesting combination of electrical and optical properties, NiO_x has been considered as active

material for various applications like energy storage, [5, 6] electrochromic smart windows, [7–11] optoelectronic devices [12], and, more importantly, dye-sensitized solar cells (DSCs) as photoactive dye-sensitized mesoporous cathode [13–19]. The utilization of NiO_x in such diverse applications has been accompanied by the development of various preparation methods and deposition techniques aimed at producing NiO_x-based materials with variable chemical composition, electrical resistivity, compactness, and morphology for performance optimization. Most common examples include sputtering [20], electrochemical deposition [21], spray pyrolysis [22] or sol–gel method [13, 23, 24]. In the present study, we have considered the fabrication of NiO_x thin films ($0.2 < l < 3$ μm) for DSC purposes through the thermal sintering of spray-deposited NiO_x nanoparticles (average diameter 40 nm) onto indium–tin oxide (ITO) substrates. The determination of the morphological, electrochemical, and photo-electrochemical properties of NiO_x films in the bare state and in the sensitized version with dye erythrosine B (ERY) [13, 24] has been accomplished together with the analysis of the electrochemical processes occurring in uncoated ITO substrates [25–27]. This approach allows for the critical evaluation of the factors regulating the performance of the DSCs based on photoactive cathodes of sintered NiO_x when deposited onto ITO through a scalable method.

2 Experimental

2.1 Deposition of NiO_x coatings

NiO_x nanoparticles, with an average particle size of 40 nm (from Sigma-Aldrich), were suspended in 2-propanol (concentration: 20 mg/mL). A loosely adherent particulate layer of NiO_x was then deposited from this suspension by spray deposition, using a technique similar to that described previously by Halme et al. [28, 29]. The nanoparticle layer was deposited onto unheated ITO-coated glass panels (5×5 cm^2) obtained from Balzers. The NiO_x nanoparticles on the conducting glass substrate were sintered for 30 min using a Carbolite Furnace (RHF 1200), in air at 450 °C [28]. This thermal treatment affords the connection of the NiO_x nanoparticles and warrants the electrical contact between nanoparticles and at the NiO_x/ITO interface. By controlling the duration of spraying, the thickness of the NiO_x nanoparticulate coatings on the ITO glass substrates was controlled as required in the range of 0.3–3 μm.

2.2 Morphology characterization equipment

The cross-sectional investigations of the NiO_x coating were carried out using a FEI Quanta 3D FEG DaulBeam™ (FEI Ltd., Hillsboro, USA) focused ion beam/scanning electron microscope (FIB/SEM) system. Before SEM analyses, the deposited NiO_x films were coated with platinum via sputtering using an Emitech K575X sputter coating unit. This was done to prevent surface charging by the electron beam.

2.3 Sensitization of NiO_x coatings

NiO_x coatings were sensitized with ERY from Sigma-Aldrich (λ_{MAX}: 535 nm), by dipping the oxide film in a 0.3 mM solution of the dye in 99.8 % ethanol (from Fisher) for 24 h at room temperature. After removing the electrode from tincture solution, the sensitized electrode was washed with pure ethanol to remove the non-chemisorbed dye molecules.

2.4 Electrochemical characterization of uncoated ITO

Before the electrochemical cycling, the uncoated ITO substrate was cleaned in an ultrasonic bath (solvent: isopropyl alcohol) for 30 min and then dried in an oven at 60 °C. After this cleaning treatment, the ITO substrate was placed in the Ar-filled glove box. The uncoated ITO substrate was manipulated in the glove-box for cell assembly.

2.5 Electrochemical characterization of NiO_x coatings

The electrochemical cell had a three-electrode configuration [30] with glass/ITO/NiO_x or dye-sensitized NiO_x as working electrode, Li rod (from Sigma-Aldrich) as counter electrode, and Li/$LiClO_4$ [0.7 M in anhydrous propylene carbonate (PC) from Fisher] as reference electrode. All potential values in this study are referred to the Li^+/Li redox couple [31]. Electrolyte was 0.7 M $LiClO_4$ in anhydrous PC. Supporting electrolyte $LiClO_4$ was purchased from Aldrich and was not pre-treated before use. Chemicals were stored in an Ar-filled glove-box (Innovative Technology, Newburyport, MA, USA), with O_2 and H_2O contents being below 10 and 5 ppm, respectively. The electrochemical cells were assembled under Ar atmosphere inside the glove-box, and a supernatant Ar atmosphere was maintained in the cell during the electrochemical experiments with bare and sensitized NiO_x samples. Cyclic voltammetries were carried out using an electrochemical analyzer (model 604C) from CH Instruments (Austin, TX, USA).

2.6 DSC preparation

The sensitized films (see Sect. 2.3) were sealed face-to-face in a sandwich configuration with a platinized fluorine-doped tin oxide (FTO) counter electrode using 30-μm-thick pre-cut Surlyn thermoplastic frame (6×6 mm^2 interior) similar to what is reported in ref [32]. The sandwiched device was filled with 0.1 M I_2 and 1.0 M LiI in

acetonitrile electrolyte through a pre-drilled hole in the counter electrode using an insertion procedure at reduced pressure [33]. The hole was sealed with Surlyn and a glass cover-slide.

3 Results and discussion

3.1 Electrochemical behavior of sintered NiO_x coating on ITO

The SEM images of a 2.7-micron-thick sample (Figs. 1, 2) demonstrate that the NiO_x coatings on ITO deposited using the spray technique, followed by furnace sintering, exhibit a relatively rough surface morphology and mesoporous features.

The NiO_x film deposited onto ITO via conventional sintering of 40 nm diameter oxide nanoparticles [28] presents a voltammogram typical of NiO_x thin coatings with two broad oxidation waves in the interval 2.75–3.75 V versus Li^+/Li [34], and lithium ions intercalation in the potential range of 1–2.5 V versus Li^+/Li [35, 36] (Fig. 3, first cycle).

Continuous cycling in the extended potential range of 1–4 V versus Li^+/Li leads to the loss of any electrochemical feature characteristic of NiO_x oxidation ($E > 2.5$ V versus Li^+/Li) and to the thorough modification of the shape of the reduction peak (Fig. 3). This indicates that n-type ITO modifies its electron transfer properties upon electrochemical cycling [37] also in non-aqueous electrolyte because of the direct contact of ITO with the electrolyte. Such a shunt effect is due to the porous nature of the sintered NiO_x coating (Figs. 1, 2), which

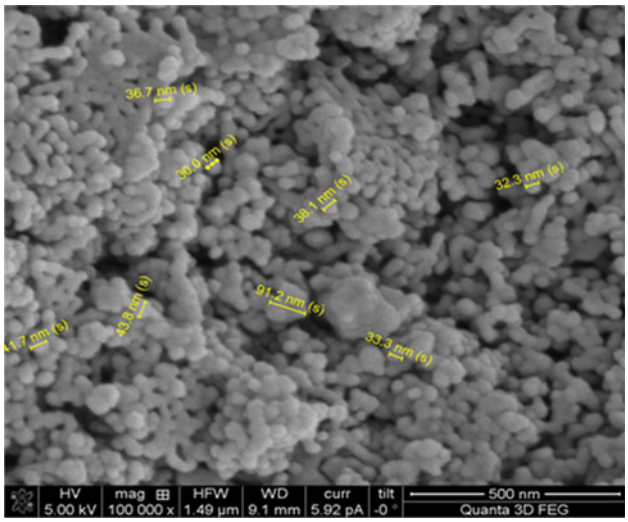

Fig. 1 SEM image showing the surface morphology of a NiO_x layer ($l = 2$–3 µm) deposited onto ITO via sintering of nanoparticles with diameter values distributed between 30 and 90 nm (evidenced in *yellow*). (Color figure online)

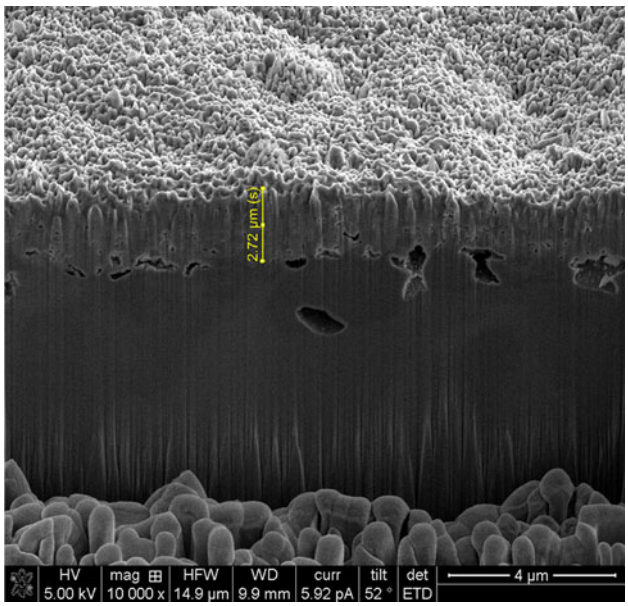

Fig. 2 Dual beam FIB–SEM image showing the cross section of a NiO_x layer ($l = 2$–3 µm) deposited onto ITO via conventional sintering of nanoparticles with average diameter of 40 nm (Fig. 1). *Yellow arrow* indicates the thickness of the NiO film. (Color figure online)

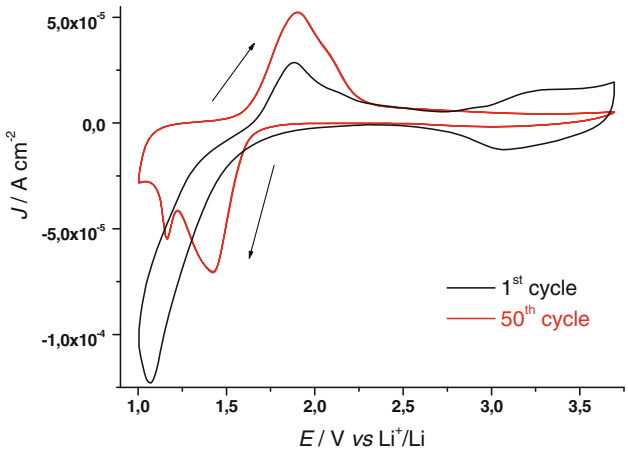

Fig. 3 Effect of electrochemical cycling on the voltammogram of NiO_x-coated ITO (scan rate: 15 mV s^{-1}). Electrolyte: 0.7 M $LiClO_4$ in anhydrous PC; counter electrode: Li; reference redox couple: Li^+/Li. Thickness of NiO_x coating: 0.3 µm

allows for the formation of the ITO/electrolyte interface. The electrochemical behavior of uncoated ITO in 0.7 M $LiClO_4$-PC (sheet resistance: 15 Ω/□, thickness: 0.1 µm) in oxygen- and water-free atmosphere has been examined within the potential window of 1.2–3.7 V versus Li^+/Li to check the electroactivity of the bare substrate. The first voltammogram of ITO (Fig. 4) presents a broad reduction peak centered at about 1.75 V versus Li^+/Li, which is accompanied by a second reduction process at about 1.2 V versus Li^+/Li (sharp peak).

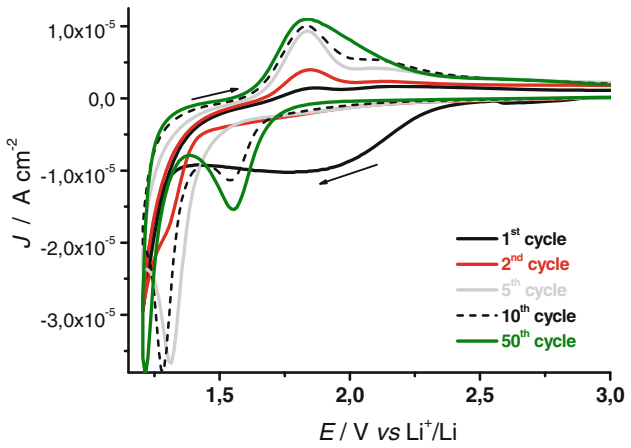

Fig. 4 Evolution of the cyclic voltammogram of ITO. Electrolyte: 0.7 M $LiClO_4$ in anhydrous PC; counter electrode: Li; reference redox couple: Li^+/Li; scan rate: 5 mV s^{-1}

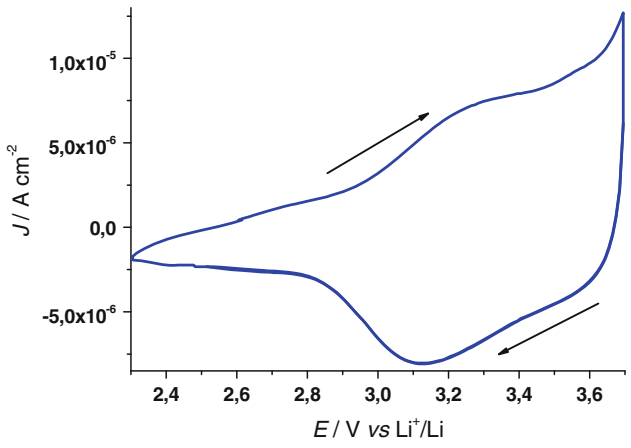

Fig. 5 Cyclic voltammogram of NiO_x coating deposited via sintering on ITO (thickness: 0.3 μm). Electrolyte: 0.7 M $LiClO_4$ in anhydrous PC; counter electrode: Li; reference electrode: Li^+/Li; scan rate: 5 mV s^{-1}

On the basis of the sole analysis of the electrochemical results, it is believed that the broad peak of reduction in the first cycle is associated with a process of lithium uptake (Eq.1) that brings about a severe rearrangement of ITO structure because of its irreversible character [27].

$$n - Sn_xIn_{2-x}O_3 + yLi^+ + ye^- \rightarrow n - Li_ySn_xIn_{2-x}O_3 \quad (1)$$

ITO lithiation (Eq. 1) is equivalent to a *n*-doping process with the occurrence of oxide reduction to a lower valence state of the metal centers. It excludes any further reduction of the metal centers to a fully reduced metallic state within the adopted range of applied potential. Beside chemical composition, the electroactivity of lithiated ITO (formula Li_y-ITO) is also modified with respect to pristine ITO as evidenced by the differences between the first and second voltammograms (Fig. 4). Upon further cycling, the quasi-reversible reduction of bare ITO shifts to 1.31 V versus Li^+/Li, and the exchange of a larger charge with respect to the second cycle is observed (Fig. 4, scan 5). Further cycling (Fig. 4, scans 10 and 50) leads to the observation of a new reduction peak at 1.54 V versus Li^+/Li the amplitude of which increases with the number of cycles. It is presumed that Li_y-ITO undergoes two distinct reduction processes consisting of lithium cations uptake at different surface sites of Li_y-ITO: the one at the higher potential should refer to the uptake of lithium ions on Li_y-ITO surface directly exposed to the electrolyte, whereas the other at the lower potential is associated with the uptake of lithium ions in correspondence of the grain borders of Li_y-ITO that are in contact with the electrolyte [10, 38, 39]. The stable voltammogram of Li_y-ITO is obtained after several hundreds of cycles and is characterized by a broad reduction wave at around 1.5 V versus Li^+/Li comprising two poorly distinguishable redox processes (see Supplementary Information, Figure SI1). Since the ITO substrate participates in reduction processes and modifies irreversibly its transport properties when its potential is comprised in the range $1.0 \leq E_{appl} \leq 2.6$ V versus Li^+/Li (Fig. 4), only the process of electrochemical oxidation of NiO_x coatings on ITO can be examined without interferences from the substrate with NiO_x oxidation occurring within $2.7 \leq E_{appl} \leq 3.7$ V versus Li^+/Li (Fig. 5). Contrary to NiO_x, the ITO substrate possesses all metal centers in the highest oxidation state [In(III) and Sn(IV)] [37], and pronounced Faradaic currents associated with the further oxidation of In and Sn in ITO are not possible upon increasing the potential further (Fig. 4). The n-type nature of the ITO substrate might impose some limitations on the rates of those oxidation reactions occurring at potentials more positive than ITO flat-band potential and generating a depletion region [40]. In fact, such a transport limitation is not verified as the sintered NiO_x thin films on highly conductive, degenerate ITO present their characteristic quasi-reversible oxidation that peaked at approximately at 3.3 V versus Li^+/Li (Fig. 5), the rate of which is limited by a NiO_x surface-confined process and not by a potential-dependent electron-transfer process through NiO_x/ITO interface (vide infra).

Such an oxidation peak presents broad features and refers to the conversion of Ni(II) into Ni(III) in the oxide film [34]. As the electrochemical reaction takes place in a solid phase, a more complete depiction of the whole redox process of NiO_x in anhydrous electrolyte with $LiClO_4$ as depolarizer could be rewritten by the following equation where ClO_4^- anion acts as charge-compensating species:

$$Ni^{(II)}_{1-y}Ni^{(III)}_{y}O_{1+y/2} + mClO_4^- \rightarrow Ni^{(II)}_{1-y-m}Ni^{(III)}_{y+m}O_{1+y/2}(ClO_4)_n + me^- \quad (2a)$$

or alternatively

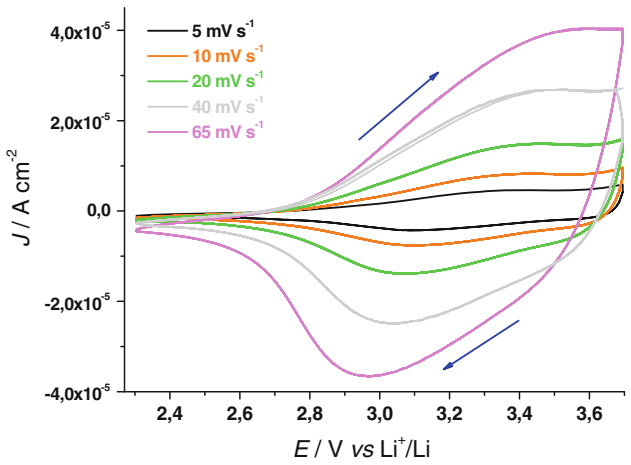

Fig. 6 Cyclic voltammograms of the NiO_x coating (thickness: 0.3 μm) deposited via sintering of NiO_x nanoparticles on ITO at different scan rates. Cell configuration is the same as in Fig. 5. *Blue arrows* indicate the direction of potential scan. (Color figure online)

$$NiO_x(OH)_m \rightarrow NiO_{x+1}(OH)_{m-1} + e^- + H^+ \quad (2b)$$

if nickel oxide is considered a mixture of oxide and hydroxide [34]. In both the cases, the electroactive NiO_x film is supposed to contain nickel ions in both the oxidation states +2 and +3. In fact, the onset of NiO oxidation is about 2.85 V versus Li^+/Li. This indicates that the pristine film of sintered NiO_x already contains a fraction of Ni(III) sites because of the open circuit voltage (V_{OC}) of the cell

$$\text{Glass/ITO/NiO}_x\text{// 0.7 M LiClO}_4\text{ in PC // Li, Ref : Li/LiClO}_4\text{(0.7 M in PC)} \quad (a)$$

is 3.07 V versus Li^+/Li, i.e., a value which is above the onset of Ni(II) site oxidation. When the scan rate dependence of the more resolved reduction peak of sintered NiO_x is analyzed (Fig. 6), a linear relationship between peak height and scan rate is found (see Supplementary Information, Figure SI4).

This corresponds to the occurrence of a surface-confined redox process [41], the rate of which does not depend on the diffusion of charge carriers or mass transfer processes (vide supra), and this is consistent with the previous data presented by Boschloo et al. [34] who examined NiO_x samples prepared via the sol–gel method.

3.2 Photo-electrochemical characterization of ERY-sensitized NiO_x

The porous nature of the NiO_x coatings deposited via sintering of oxide nanoparticles (Fig. 1) renders possible the efficacious sensitization of the oxide with a visible light absorber. In the present study, erythrosine B (ERY) has been considered as dye sensitizer because of the matching of its frontier energy levels with the band edges of p-type NiO_x. [13, 24, 28, 42] Dye sensitization of the sintered NiO_x sample with ERY generally leads to a small decrease of the dark current densities (Fig. 7), with respect to the corresponding curves of bare nickel oxide samples (Fig. 6). Moreover, current peaks associated with ERY-based electrochemical processes are not introduced in the voltammogram of ERY-sensitized NiO_x deposited on ITO substrates within the experimental range of applied potential.

Therefore, ERY layer behaves as an electrochemically inert layer, with no involvement in any of the observed faradic processes. Illumination of the dye-sensitized oxide samples with white light produces a positive photo-potential, an increase of the oxidation current density, and the negative shift of the current baseline when no redox processes occur (Fig. 7). These facts can be explained in terms of photogeneration of positive charge carriers in dye-sensitized nickel oxide when visible light is absorbed by ERY layer (photoconductive effect) [13, 24, 42]. Cyclic voltammetries of ERY-sensitized NiO_x have been carried out at different scan rates in the dark and under white light illumination (see Supplementary Information, Figures SI5 and SI6) to evaluate the characteristics of the dark and photo-oxidation process of NiO_x when sensitized.

The cathodic peak referring to the reverse process $Ni^{(III)} \rightarrow Ni^{(II)}$ (reverse of processes in Eq.2) has been considered for analysis because of its generally better resolution with respect to the correlated anodic peak which displays broader features in the voltammogram. Similar to bare NiO_x, both the dark and photo-electrochemical oxidation processes of ERY-sensitized NiO_x present the typical features of a surface-confined redox process being the current peaks directly proportional to the scan rate (see Supplementary Information, Figure SI7).

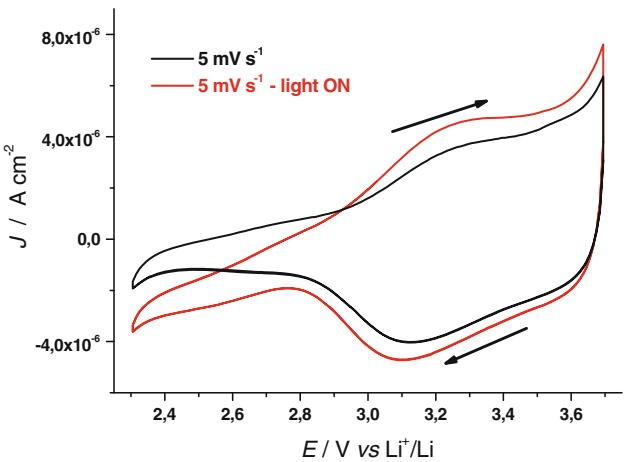

Fig. 7 Cyclic voltammograms the of ERY-sensitized NiO_x coating (thickness: 0.3 μm) in the *dark* and under illumination with *white light* (P_{in} = 50 W) from a halogen lamp. Electrolyte composition as in Fig. 5. Electrode area: 1.75 cm^2. *Arrows* indicate the direction of potential scan

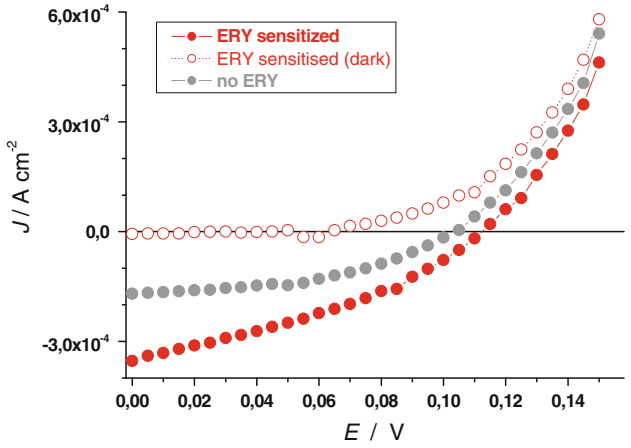

Fig. 8 Characteristic *J–V* curves of cathodic DSCs in I_3^-/I^- electrolyte for NiO_x in different states and conditions: (i) bare state under illumination; (ii) ERY-sensitized state under illumination; (iii) ERY-sensitized state in the dark. Electroactive area: 0.5–0.7 cm^2. The incident intensity of the sun simulator was 0.1 W cm^{-2}. Prior to sensitization, the thickness of the NiO_x coating was 0.6 μm

ERY-sensitized NiO_x on ITO has been utilized as photoactive electrode in a cathodic DSC [24] with platinized FTO as counter electrode. The photocathode and the counter electrode had the same electroactive area in the DSC. The electrolyte was a solution of the redox couple I_3^-/I^- in acetonitrile. The characteristic curve of the NiO_x-based cathodic DSC is presented in Fig. 8.

The cathodic DSC based on photoactive-sintered NiO_x showed an overall efficiency $\eta = 0.014$ % with open circuit voltage, $V_{OC} = 0.11$ V, short circuit current density, $J_{SC} = -0.353$ mA cm^{-2}, and fill factor, FF = 0.35. The influence of sensitization can be evaluated through the comparison of the characteristic curves recorded on illuminated NiO_x samples with and without sensitizer (Fig. 8). The resulting variations, ΔV_{OC} and $\Delta J_{SC,}$, in passing from the performance of bare NiO_x to that of ERY-sensitized NiO_x, are, respectively, 9 mV and -1.83×10^{-4} A cm^{-2}. These results indicate that sensitization has a stronger influence on the kinetics-dependent term J_{SC} with respect to the thermodynamic parameter V_{OC}. It must be pointed out that the performance of bare NiO_x is comparable to that of the ERY-sensitized cathode (Fig. 8). This implies that the photogeneration of charge carriers in bare NiO_x following the absorption of the UV fraction of the impinging radiation [22] has non-negligible effects. The sole effect of illumination is evaluable when the characteristic curves recorded on ERY-sensitized NiO_x in the dark and under illumination (Fig. 8) are confronted. The parameter V_{OC} has an increment of 50 mV, whereas the cathodic J_{SC} has an increase in module of 3.47 A cm^{-2} upon illumination of the cathodic DSC with 0.1 W cm^{-2} of sun simulator light. These results show a considerable improvement of the *J–V* characteristic curve if compared to that of sol–gel-prepared NiO_x films sensitized with the same dye [13], which gave $V_{OC} = 0.083$ V, $J_{SC} = -0.2$ mA cm^{-2}, FF = 0.27, and $\eta = 0.0076$ % when 1-μm-thick NiO_x was tested. The improvements here reported are mainly ascribed to the better efficiency of sensitization in the NiO_x films obtained from the sintering of nanoparticles as a consequence of the enhanced mesoporosity (Figs. 1, 2) with respect to thin films of the same material prepared with wet methods [14, 21, 23].

4 Conclusions

This study has examined the electrochemical properties of NiO_x coatings ($l < 3$ μm) on ITO, obtained using nanoparticle spray deposition/furnace-sintering treatment. NiO_x coatings prepared via sintering of nanoparticles present a mesoporous morphology as a consequence of the nanoparticulate geometry retained after the thermal treatment. The oxidation of bare NiO_x coatings (solid state redox process) is not diffusion controlled but surface confined. It has been proven that the ITO substrate can get involved in cathodic redox processes that alter irreversibly the process of charge transfer through the ITO/NiO_x interface. For this reason, the sole process of NiO_x electrochemical oxidation can be driven in the absence of ITO substrate interference within the potential range of $2.7 \leq E_{appl} \leq 3.7$ V versus Li^+/Li. After sensitization with commercial erythrosine B, the photo-electrochemical properties of the modified NiO_x coatings were analyzed for consideration of application in cathodic DSCs. Again, in the sensitized state, the oxidation of NiO_x is a surface-confined process which is not modified by the presence of a monolayer of dye. The NiO_x-based DSCs displayed an improved *J–V* performance with respect to NiO_x samples sensitized with the same dye but prepared with wet, not scalable methods displaying an overall efficiency, $\eta = 0.014$ versus 0.008 % of sol–gel sample. The improvements obtained in this study are mainly ascribed to the better efficiency of sensitization as a consequence of the enhanced mesoporosity of NiO_x films obtained using nanoparticle spray deposition followed by furnace sintering process.

Acknowledgments This article is based on studies supported by the Science Foundation Ireland for the Solar Energy Conversion Strategic Research Cluster under Grant No. [07/SRC/B1160]. The authors acknowledge the assistance and support of industry partner, Celtic Catalysts Ltd.

References

1. Nalage SR, Chougule MA, Shashwati S, Joshi PB, Patil VB (2012) Thin Solid Films 520:4835
2. Morrison SR (1980) Electrochemistry at semiconductor and oxidized metal electrodes. Plenum Press, New York

3. Sato H, Minami T, Takata S, Yamada T (1993) Thin Solid Films 236:27
4. Granqvist CG (2007) Sol Energy Mater Sol Cells 91:1529
5. Nam KW, Yoon WS, Kim KB (2002) Electrochim Acta 47:3201
6. Lang JW, Kong LB, Liu M, Luo YC, Kang L (2010) J Solid State Electrochem 14:1533
7. Estrada W, Andersson AM, Granqvist CG, Gorenstein A, Decker F (1991) J Mater Res 6:1715
8. Svegl F, Surca-Vuk A, Hajzeri M, Slemenik-Perse L, Orel B Sol (2012) Energy Mater Sol Cells 99:14
9. Avendaño A, Azens A, Niklasson GA, Granqvist CG (2007) Mater Sci Eng B 138:112
10. Huang H, Tian J, Zhang WK, Gan YP, Tao XY, Xia XH, Tu JP (2011) Electrochim Acta 56:4281
11. Gillaspie D, Norman A, Tracy CE, Pitts JR, Lee SH, Dillon A (2010) J Electrochem Soc 157:H328
12. Irwin MD, Buchholz DB, Hains AW, Chang RPH, Marks TJ (2008) Proc Nat Acad Sci 105:2783
13. He J, Lindstrom H, Hagfeldt A, Lindquist SE (1999) J Phys Chem B 103:8940
14. Nakasa A, Usami H, Sumikura S, Hasegawa S, Koyama T, Suzuki E (2005) Chem Lett 34:500
15. Morandeira A, Boschloo G, Hagfeldt A, Hammarström L (2008) J Phys Chem C 112:9530
16. Nattestad A, Ferguson M, Kerr R, Cheng YB, Bach U (2008) Nanotechnology 19:295304
17. Qin P, Zhu H, Edvinsson T, Boschloo G, Hagfeldt A, Sun L (2008) J Am Chem Soc 130:8570
18. Li L, Gibson EA, Qin P, Boschloo G, Gorlov M, Hagfeldt A, Sun L (2010) Adv Mater 22:1759
19. Nattestad A, Mozer AJ, Fischer MKR, Cheng YB, Mishra A, Bauerle P, Bach U (2010) Nature Mater 9:31
20. Awais M, Rahman M, MacElroy JMD, Coburn N, Dini D, Vos JG, Dowling DP (2010) Surf Coat Technol 204:2729
21. Wu MS, Wang MJ (2010) Chem Commun 46:6968
22. Garduño IA, Alonso JC, Bizarro M, Ortega R, Rodríguez-Fernández L, Ortiz A (2010) J Cryst Growth 312:3276
23. Jiao Z, Wu M, Qin Z, Xu H (2003) Nanotechnology 14:458
24. He J, Lindstrom H, Hagfeldt A, Lindquist SE (2000) Sol Energy Mater Sol Cells 62:265
25. Cogan SF, Anderson EJ, Plante TD, Rauh RD (1985) Appl Opt 24:2282
26. Bressers PMMC, Meulenkamp EA (1998) J Electrochem Soc 145:2225
27. Wang Z, Hu X (2001) Thin Solid Films 392:22
28. Awais M, Rahman M, MacElroy JMD, Dini D, Vos JG, Dowling DP (2011) Surf Coat Technol 205:S245
29. Halme J, Saarinen J, Lund P (2006) Sol Energy Mater Sol Cells 90:887
30. Decker F, Passerini S, Pileggi R, Scrosati B (1992) Electrochim Acta 37:1033
31. Masetti E, Dini D, Decker F (1995) Sol Energy Mater Sol Cells 39:301
32. Gibson EA, Smeigh AL, Le Pleux L, Fortage J, Boschloo G, Blart E, Pellegrin Y, Odobel F, Hagfeldt A, Hammarström (2009) Angew Chem Int Ed 48:4402
33. Mastroianni S, Lanuti A, Penna S, Reale A, Brown TM, Di Carlo A, Decker F (2012) ChemPhysChem, to be published
34. Boschloo G, Hagfeldt A (2001) J Phys Chem B 105:3039
35. Passerini S, Scrosati B, Gorenstein A (1990) J Electrochem Soc 137:3297
36. Passerini S, Scrosati B (1994) J Electrochem Soc 141:889
37. Armstrong NA, Lin AWC, Masamichi F, Kuwana T (1976) Anal Chem 48:741
38. Chippindale AM, Dickens PG, Powell AV (1991) Prog Solid St Chem 21:133
39. Whittingham MS, Chen R, Chirayil T, Zavalij P (1997) Solid State Ionics 94:227
40. Gerischer H (1990) Electrochim Acta 35:1677
41. Bard AJ, Faulkner LR (2001) Electrochemical methods (fundamentals and applications), 2nd edn. John Wiley, New York, p 595
42. Vera F, Schrebler R, Munoz E, Suarez C, Cury P, Gomez H, Cordova R, Marotti RE, Dalchiele EA (2005) Thin Solid Films 490:182